This is a preprint of a non-peer-reviewed article, submitted to Journal of Climate on 5 June 2025.

The spatio-temporal variability, trends, and drivers of winter Arctic polynyas

Carmen Hau Man Wong, [a] Céline Heuzé,[a] Luisa Ickes, [b] and Lu Zhou [c]

[a] *Department of Earth Sciences, University of Gothenburg, Sweden*

[b] *Department of Space, Earth, and Environment, Chalmers University of Technology, Sweden*

[c] *Institute for Marine and Atmospheric research Utrecht, Utrecht University, The Netherlands*

Corresponding author: Carmen Hau Man Wong, hau.man.wong@gu.se

ABSTRACT: Polynyas, thin-ice or open water regions within the sea ice, have regularly been observed in the Arctic since satellite observations began in the 1970s. Their opening, in response to complex interactions between several drivers, significantly influences the regional weather and climate, ecosystem, and the global ocean. Yet their monitoring at the pan-Arctic scale is rare since their detection is not trivial. Here, we use three sea ice satellite data products to detect and investigate all Arctic polynya events since 1978, focusing on their winter locations and total area. We compute the polynyas' recurrence percentage, total number and area, varying the sea ice concentration (30 – 60%) and thickness (10 – 30 cm) thresholds to enhance our analysis robustness. We find that the most active polynya regions are along the coasts of the Laptev Sea, Kara Sea, Franz-Josef Land, northwestern Greenland, Beaufort Sea and Chukchi Sea. Both total and cumulative polynya areas have significant increasing trends in these regions and at the pan-Arctic scale between 1978-2024. In these regions, we find consistent positive correlations for atmospheric drivers (air temperature and wind speeds) with polynya openings and area, along with a strong increase in air temperature and a weak increase in extreme wind events. Temperature is correlated with polynya area extent and wind variables with polynya opening in most regions. Under rising temperatures and stronger extreme winds, our results suggest an increase in Arctic polynya activity, although polynyas might then extend into the open ocean, where different processes would drive their opening.

1. Introduction

Polynyas, open water regions within the sea ice cover, are essential for deep water formation and air-sea surface energy exchanges in polar regions. Since satellite passive microwave observations became available in polar regions four decades ago, this natural phenomenon has been observed regularly in the open ocean and coastal areas (Gordon and Comiso 1988; Preußer et al. 2016). Polynyas were classified into two major types in early studies: coastal (latent heat) polynyas and open-water (sensible heat) polynyas. Coastal polynyas form where there are divergent ice motions driven by dynamical drivers (e.g. wind, ocean currents), usually along the coast (Smith et al. 1990; Morales Maqueda et al. 2004). Meanwhile, open-water polynyas form away from the coast due to abnormal thermodynamic drivers (e.g. oceanic heat intrusion), causing sea ice to melt at the ocean surface (Smith et al. 1990; Morales Maqueda et al. 2004). In addition, it is possible that mechanical and thermal forcings have similar contributions to the polynya formation, and this type is therefore called hybrid latent and sensible polynyas (Hirano et al. 2016). Most Arctic polynyas are coastal polynyas, known for their high ice production on-site (Tamura and Ohshima 2011). Polynyas expose the relatively warm water surface to cold air, and the strong heat loss from the ocean to the atmosphere causes subsequent ice refreeze (Morales Maqueda et al. 2004). This sea ice production enhances the upper ocean salinity via brine rejection; polynyas are therefore crucial for deep water formation (Aagaard et al. 1981; Martin and Cavalieri 1989). The vigorous air-sea interaction also modifies the surface heat and moisture budgets, intensifying the local turbulent mixing, influencing regional atmospheric dynamics, and promoting Arctic cloud formation (Gultepe et al. 2003; Boisvert et al. 2012; Monroe et al. 2021). In addition, biogeochemistry processes are also affected by polynya openings, with more gaseous exchange in winter and primary productivity in early spring at the open water surface (Else et al. 2013; Marchese et al. 2017; Moore et al. 2023). To better understand the causes and impacts of polynyas, it is essential to study their precise locations in the Arctic. However, these locations may change: The Arctic has been significantly warming, nearly four times faster than rest of the world (Rantanen et al. 2022). The rise of the surface temperature is consistent with recent sea ice reductions, while local and regional wind trends are more inconsistent. In an increasingly uncertain Arctic climate, it is crucial to establish with more certainty the relationship between winter Arctic polynyas and their drivers, else polynya events may become more unpredictable in the future.

Early Arctic polynya research relied mainly on passive microwave satellite-retrieved sea ice concentration (SIC), as they are ground-truthed data with good spatial and temporal coverage (Martin and Cavalieri 1989; Cavalieri and Martin 1994; Bareiss and Görgen 2005). The data are on a daily scale, regardless of nighttime or dense cloud cover, which permits their observation even in polar winter (Tamura and Ohshima 2011). With the improvement of satellite measurements, recent polynya research has put more emphasis on thin sea ice thickness (SIT) retrieval as ice production and salt flux at polynya sites can be quantified at the same time (Tamura and Ohshima 2011; Iwamoto et al. 2014; Preußer et al. 2016). These studies however often focus on the regional scale by the Arctic coast, predominantly along the Laptev coast, Canadian coast, and Chukchi coast, where polynyas recur almost every year and concurrent in-situ data (e.g moorings) are available (Ingram et al. 2002; Willmes et al. 2011; Hirano et al. 2016). Long-term, pan-Arctic polynya research is still rare. The last pan-Arctic polynya mapping was conducted more than a decade ago by Preußer et al. (2016), covering the period 2002-2015, with the objective of quantifying ice production rather than investigating polynya dynamics. Here we not only conduct an updated pan-Arctic polynya mapping, but also quantify trends in this crucial natural phenomenon using satellite-retrieved winter sea ice concentration and thickness during the period 1978-2024. Furthermore, to explain the trends that we observe in the different regions of the Arctic Ocean, we determine the relationship between polynya openings and total area and their atmospheric drivers.

Section 2 describes the sea ice satellite products and atmospheric data used in this study. Section 3 describes our novel Arctic polynya detection method and the methodology for the calculated results and climate variables. Section 4 presents the spatial and temporal polynya trends from a pan-Arctic to regional perspective, as well as the analysis of their atmospheric drivers. We then briefly summarise our results and add concluding remarks in section 5.

2. Satellite products and atmospheric reanalysis data

a. Sea Ice Concentration (SIC)

We use two daily SIC datasets from the National Snow and Ice Data Center (NSIDC) and the University of Bremen Sea Ice Remote Sensing group (Table 1). The data are accessible online at the NSIDC (`https://nsidc.org/data/nsidc-0051/versions/2`) and the University of Bremen Sea Ice Remote Sensing websites (`https://seaice.uni-bremen.de/start/`). NSIDC SIC data are derived from Nimbus-7 Scanning Multichannel Microwave Radiometer (SMMR) and the Defense Meteorological Satellite Program (DMSP) Special Sensor Microwave/Imager (SSM/I) – Special Sensor Microwave/Imager/Sounder (SSMIS). The multichannel satellites of these observation programs measure the frequency from 6 GHz to 91 GHz horizontally and vertically (NSIDC 2024). The raw data are then processed by the NASA Team algorithm, using the horizontal and vertical polarization of the 18/19 GHz channel, as well as the vertical gradient ratio between frequencies of 18/19 GHz and 37 GHz (Cavalieri et al. 1984; Comiso et al. 1997; Cavalieri et al. 1999). This SIC product has a daily temporal coverage from 1978 to 2024 with a 25 km spatial resolution.

The other SIC dataset that we use is obtained from the University of Bremen Sea Ice Remote Sensing group. It is derived from the brightness temperature T_B data captured by the Advanced Microwave Scanning Radiometer-EOS (AMSR-E) and the Advanced Microwave Scanning Radiometer 2 (AMSR2) (Spreen et al. 2008). It has an observation period from 2002 to 2024, during which there is a 9-month data gap between 2011 – 2012 (Spreen et al. 2008). AMSR-E and AMSR2 take measurements in six frequency bands from 6.9 to 89 GHz. SIC is derived from the ARTIST Sea Ice algorithm using 89 GHz data, which has a higher spatial resolution than the NASA Team algorithm (Spreen et al. 2008). The SIC retrieval algorithm also resolves the influences of clouds and water vapor by introducing weather filters which are calculated from data at 18, 23 and 37 GHz channels (Spreen et al. 2008). The retrieved SIC is provided on 6.25×6.25 km grid cells.

b. Thin Sea Ice Thickness (SIT)

The SIT product that we use, which is provided by the University of Bremen Sea Ice Remote Sensing group, is derived from the spaceborne passive microwave sensors Soil Moisture Ocean Salinity (SMOS) and Soil Moisture Active Passive (SMAP) brightness temperature data at 1.4 GHz (L-band, Huntemann et al. 2014; Tian-Kunze et al. 2014; Paţilea et al. 2019, see Table 1). The SMOS measurements started in 2010, providing more than ten years of T_B data for SIT retrieval thus far. The SMOS SIT is retrieved from an empirical algorithm by Huntemann et al. (2014), utilizing the L-band at incident angles of 40° and 50°. After SMAP was launched in 2015, a novel SIT retrieval algorithm combining T_B data from SMOS and SMAP was derived by Paţilea et al. (2019). The SMOS-SMAP algorithm complements the original SMOS algorithm by Huntemann et al. (2014) as SMOS-SMAP T_B data has a 6% increase of spatial coverage (Paţilea et al. 2019). This combined daily SIT dataset covers the period 2010 - 2024 with a 12.5 km spatial resolution. In general, SIT is retrieved up to 50 cm; most research agrees that 50 cm is the maximum ceiling to have reliable SIT results and a reasonable uncertainty range (Kaleschke et al. 2012; Huntemann et al. 2014; Paţilea et al. 2019).

Table 1. Summary of the passive microwave-based satellite product datasets used in this study.

Satellite Data Product	Spaceborne Sensor	Temporal Coverage (Resolution)	Spatial Resolution	Data Range
Sea Ice Concentration	SMMR, SSM/I and SSMIS	1978 - 2024 (Daily)	25 km	0 - 100%
	AMSR-E and AMSR2	2002 - 2011 (Daily, AMSR-E) 2012 - 2024 (Daily, AMSR2)	6.25 km	
Sea Ice Thickness	SMOS and SMOS-SMAP	2010 - 2024 (Daily)	12.5 km	0 - 50 cm

c. Atmospheric drivers

We use the European Centre for Medium-Range Weather Forecasts Reanalysis version 5 (ERA5) hourly data for our trend and climatology analyses of the potential polynya drivers (Hersbach et al. 2020). ERA5 data have a spatial resolution of $0.25° \times 0.25°$, which is in the Arctic is roughly equivalent to 25 km $\times$ 25 km. Given that the satellite products in this study have a daily temporal resolution, we use the hourly data at the 00:00, 06:00, 12:00, and 18:00 time stamps, averaging them to produce a daily mean value. The precise values of hourly atmospheric data are not critical in our overall trend analysis, and the diurnal cycle of the Arctic Ocean in the polar winter is negligible. Most Arctic polynyas have been identified as coastal or hybrid polynyas in previous studies (e.g. Tamura and Ohshima 2011; Ren et al. 2022), which means that wind is an essential factor driving polynyas to open. Meanwhile, Pease (1987) found that the near-surface air temperature has a strong impact in determining the size of a polynya. Therefore, we use the 2m air temperature (T2m), 10m u-component of wind (U10), 10m v-component of wind (V10), and the wind speed (WS) computed from U10 and V10, to try to explain polynya activity in the Arctic.

3. Arctic polynya retrieval

a. Data analysis period

The data analysis period is based on the availability of the three satellite datasets we just described: 1978 – 2024 (SMMR, SSM/I & SSMIS), 2002 – 2024 (AMSR-E & AMSR2), and 2012 – 2024 (SMOS & SMOS-SMAP). We only analyse polynyas formed in wintertime for each year. Previous research has identified that the Arctic freeze up day is in September-October, and the melt onset is in May (Markus et al. 2009; Bliss and Anderson 2018). Thus, in this study, we define the winter period from November to April as the sea ice cover is most stable then. Due to an observation gap between AMSR-E and AMSR2, the 2011/12 winter is skipped for the AMSR-E & AMSR2 SIC results. As we explain in the next section, our SIT-based polynya retrieval requires concurrent AMSR-E & AMSR2 data, so we do not show SMOS & SMOS-SMAP results for the 2011/2012 winter either. Besides, we did not process SMOS & SMOS-SMAP data in the 2010/11 winter because of the large areas with missing data within the study region.

b. Polynya detection each winter

The polynya detection algorithm is summarised in Figure 1. We separate the sea ice regions from open oceans and land with a flood-fill algorithm. Due to the geometry of the Arctic, the flood-filling has to be initiated with several seeds in the open Atlantic and Pacific oceans (Figure 1a, orange stars). The algorithm masks grid cells below a certain sea ice threshold as being part of the open ocean, filtering out the sea ice cover. The study area is then limited to latitudes 65° – 90°N, and only open water regions within the sea ice cover are analysed (Figure 1b). In the next step we apply a SIC or SIT threshold to the analysis region: Grid cells with values below the threshold will be defined as open water (potential polynyas), and those above as sea ice (Figure 1c). Threshold values are determined by a sensitivity test, as we describe in the next subsection. Finally, we want to ensure that the potential polynyas are within the sea ice cover, where the maximum extent is usually defined as SIC $\geq$ 15%. For the SIC products, the SIC threshold range is always above 15%. For the SIT products, we need an extra step and keep only the SIT grid cells where SIC is above 15%, i.e. within the sea ice extent. To do so, we downgrade the spatial resolution of the AMSR-E/AMSR2 SIC data from 6.25 km to 12.5 km to match the SIT product's horizontal resolution. If any potential polynya as detected by SIT is outside the sea ice extent from the downgraded AMSR-E/AMSR2, it is removed from the results (Figure 1d).

We create a base map to indicate all the polynya locations for each day. We use the `label()` function from the Python `scipy` package (Virtanen et al. 2020) to count the cumulative number of polynyas on the base map. This function considers grid cells that are adjacently connected and diagonally connected as part of the same polynya. From daily base maps we generate winter base maps, and calculate the recurrence percentage at each grid cell. High recurrence percentage means high polynya activity. We use the recurrence percentage maps to investigate the polynya spatial distribution across the Arctic for the last 46 winters. For pan-Arctic and regional analyses, we also compute polynya area time series. The cumulative winter polynya area is the sum of all open-water grid cells across the study region on the daily base map for one winter; the total winter polynya area is the sum of all grid cells that have been identified at least once as a polynya in one winter.

c. Sea ice threshold sensitivity test

SIT and SIC are each sensitive to different ice processes and their products have different resolutions and observation periods. Therefore, it is essential to determine a SIC-SIT threshold pair to make our results consistent over their common time period (i.e. after 2010). We conduct a sensitivity test on the downscaled AMSR-E & AMSR2 SIC (12.5km), used to determine whether SIT retrieved polynyas are inside the sea ice extent each day (see previous subsection), and the SMOS & SMOS-SMAP SIT dataset. Theoretically, the cumulative polynya area of each winter extracted by SIC and SIT should be the same. SIC and SIT will not have the same values in practice due to different satellite sensors, frequency bands and retrieval algorithms. Therefore, we calculate the area differences of SIC and SIT to decide which threshold pairs have the least deviation in area. We compute the winter cumulative polynya area over the common time period (2012-2024) using the different thresholds mentioned in the literature (Table 2): We vary the SIC thresholds from 30% to 60% with an interval of 10%, and the SIT thresholds from 10 cm to 30 cm with an interval of 5 cm. The SIC-SIT threshold pair with the smallest area deviation can produce consistent results. The averaged yearly area differences are then normalised relative to 0, which is the most ideal case without area differences between SIC and SIT. The normalised results are presented in Figure 2. As expected, some pairs have differences close to or of 1, i.e. are impossible, for example thick sea

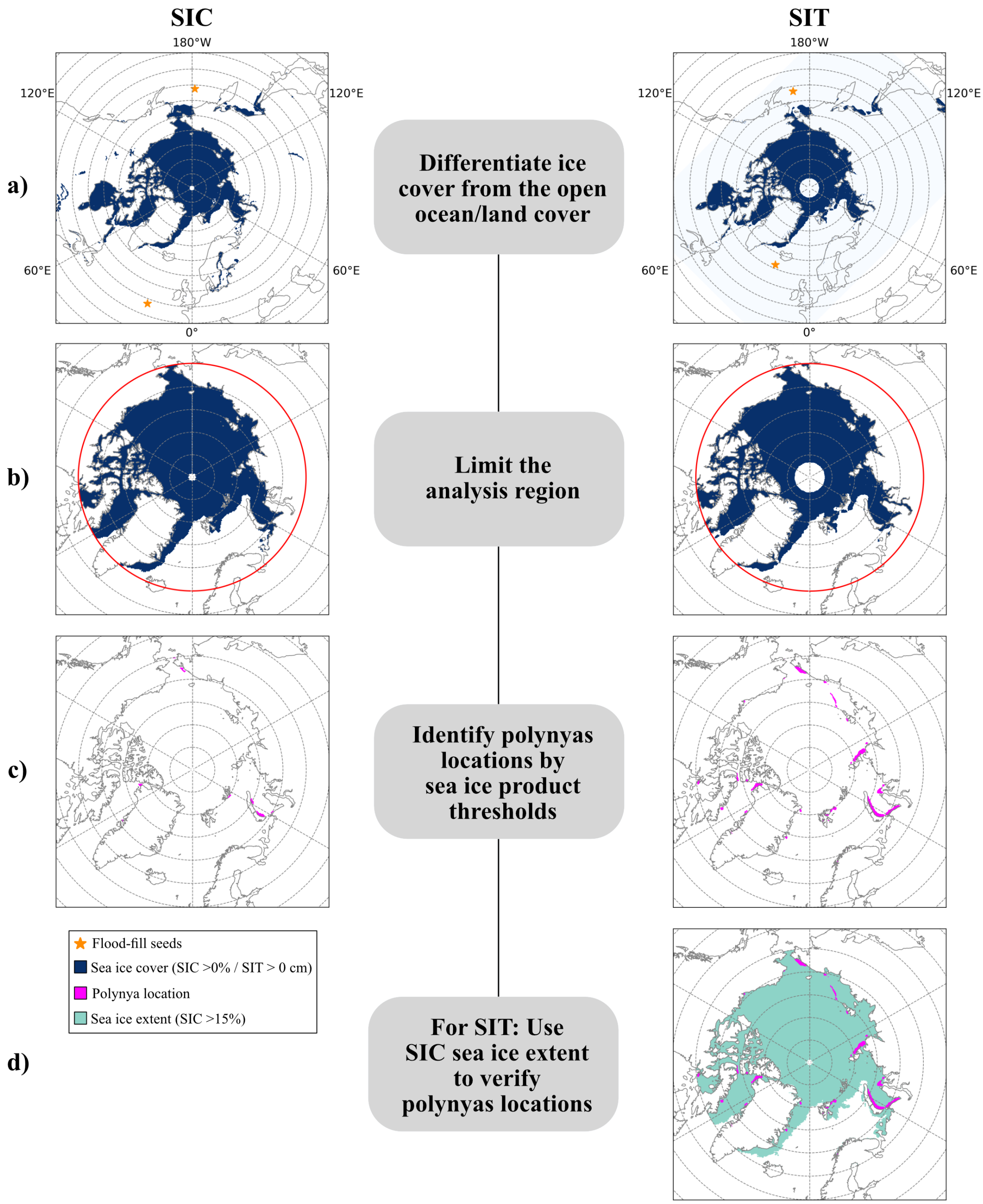

FIG. 1. Flowchart of the polynya detection process: (a) Use a flood-fill algorithm to separate sea ice and open ocean and land; (b) Limit the analysis region to 65° - 90°N; (c) Identify potential polynya locations using our detection algorithm with specific sea ice product thresholds; (d) An extra step for SIT: use SIC 15% sea ice extent to verify polynya locations.

ice but low concentration. Similarly, thin ice with a high concentration returns an error of nearly 0.5. The pair with the the smallest cumulative area difference is 50% SIC and 20 cm SIT (error of 0.03). This threshold pair is also the most prevalent threshold option in earlier studies (Table 2). Therefore, 50% SIC and 20 cm SIT is the one we choose for the rest of our analysis.

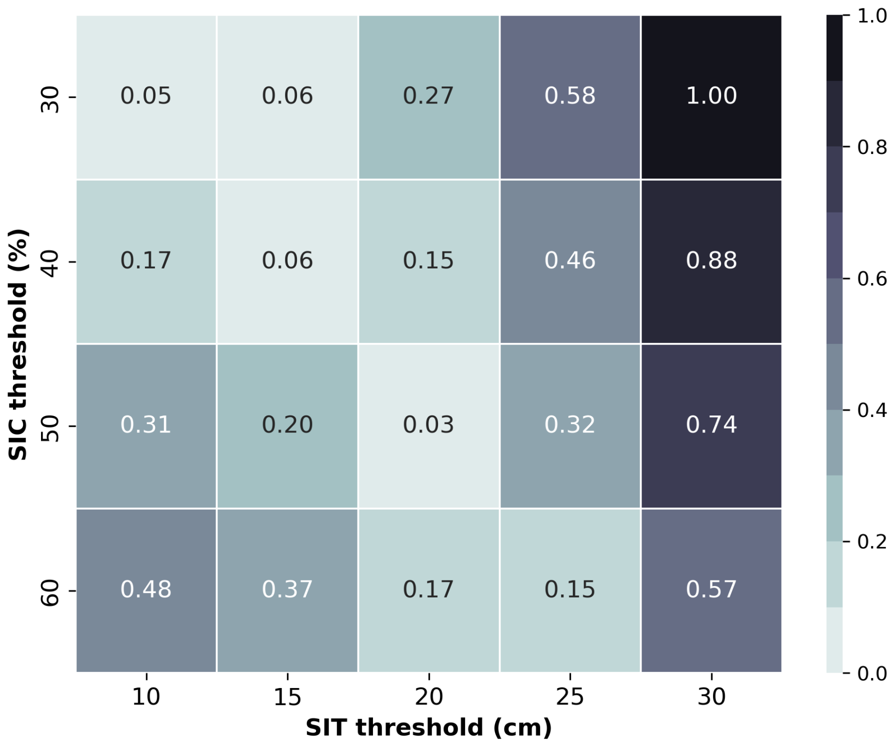

Fig. 2. Sea ice product threshold sensitivity results. Normalised values represent the averaged yearly area differences between SIC and SIT retrieval results.

Table 2. Summary of SIC/SIT thresholds applied in previous Arctic or Antarctic polynya studies.

Sea Ice Products	Threshold	Reference
SIT	10 cm	Martin et al. (2004)
	12 cm	Nakata et al. (2015); Mohrmann et al. (2021)
	15 cm	Tamura and Ohshima (2011)
	20 cm	Martin et al. (2004); Adams et al. (2013); Preußer et al. (2015, 2016); Ren et al. (2022)
	25 cm	-
	30 cm	Smedsrud et al. (2006)
SIC	30 %	Kawaguchi et al. (2011); Tamura and Ohshima (2011); Mohrmann et al. (2021)
	40 %	Campbell et al. (2019)
	50 %	Dokken et al. (2002); Campbell et al. (2019); Shen et al. (2021); Bennett et al. (2024)
	≥60 %	Massom et al. (1998); Campbell et al. (2019); Monroe et al. (2021); Zhou et al. (2022)

d. Trends and driver analysis in the polynya regions

We examine the evolution of all winter Arctic polynyas and, for each region, the correlation with atmospheric variables potentially driving this evolution across the study period. To do so, we determine the specific regions of interest by computing the polynya recurrence percentage of the spatial distribution map for each satellite dataset, for the observation period of that dataset. Then a general area is identified both visually as having a high recurrence percentage (purple regions) but also based on regions frequently studied in previous research (listed in Table 2). We quantify the trend in polynya opening frequency (i.e. opening recurrence for each winter), total polynya area and cumulative polynya area by linear least-squares regression over the entire dataset period for the pan-Arctic and regional values.

To explain the trend results, we perform a lagged correlation analysis between the daily on-off opening state or the daily total polynya area with atmospheric variables, using the Pearson correlation. The on-off state of a polynya grid cell indicates whether, on that day, the polynya is open (value of 1) or closed (0). We also compute the trends for all four atmospheric variables, using the same method as for the polynyas. The time for a winter polynya to form and become stable typically takes between half a day and 4 days, which implies that there is a time lag for atmospheric forcings to impact the development of a polynya (Pease 1987). Thus, we perform a lagged correlation analysis, with a slightly longer time lag of up to 7 days. We test both instantaneous and lagged correlation to investigate the lag effect of atmospheric variables on polynyas, with atmospheric variables as the lead-lag parameter since they are the suspected drivers of polynya opening. For each grid, we calculate the correlation coefficient for all lag days and select the day with the highest absolute coefficient value to represent the time with the most significant lag effect. After that, we obtain the total number of grid cells for each lag day. All results presented are statistically significant at or above the 90% level, verified by Student t-tests.

4. Results and Discussion

a. Spatial distribution of Arctic winter polynyas

The Arctic polynya recurrence for all years is consistent among all three satellite products, showing that most polynyas are formed along coastlines (Figure 3). All satellite products result in 50% or more recurrence in the east of Svalbard (including Storfjorden, region 1 on Figure

3a), Franz Josef Land (region 2), the western Kara Sea (East of Novaya Zemlya, region 3), the western Laptev Sea (region 4), the Chukchi Sea (region 6), the eastern Beaufort Sea (region 7) and the North Open Water region (NOW, region 8). Spatial patterns are consistent, but the recurrence magnitude differs between products due to their different spatial resolutions and time periods. Note that most of these purple regions along the coast have previously been identified as major Arctic polynyas, in terms of high ice production rate, by previous studies that applied different retrieval methods based on radiation emission (Tamura and Ohshima 2011; Iwamoto et al. 2014; Preußer et al. 2016). More locations are identified as polynyas by our algorithm when the spatial resolution of the sea ice product increases: 63.6% of the grid cells have a non-zero polynya frequency in the 6.25 km resolution AMSR-E & AMSR2; 57.4% in the 12.5 km SMOS & SMAP; and 21.5% in the 25 km SMMR, SSM/I & SSMIS. AMSR-E & AMSR2 (Figure 3b) and SMOS & SMOS-SMAP results (Figure 3c) both reveal a band of strong polynya activity from east of Greenland to north of Svalbard, a location close to the ice edge. Our algorithm differentiates polynyas from the sea ice edge using a SIC threshold of 15%, yet the possibility remains that noise from the marginal ice zone (MIZ) is incorrectly identified as polynyas. There is a considerable uncertainty exceeding 10% in MIZ retrieval in satellite observation, according to Rolph et al. (2020), and thus high resolution data may overestimate polynya recurrence near the ice edge.

The length of the satellite data period also influences the spatial patterns observed in Figure 3. Since SMMR, SSM/I & SSMIS has the longest SIC period (47 years), locations with low (Figure 3a, yellow - orange) and high recurrence (purple) are more distinguishable than for AMSR-E & AMSR2 (Figure 3b) and SMOS & SMOS-SMAP (Figure 3c). All three results show the major polynyas; however, in the Laptev Sea and the Kara Sea regions, the AMSR-E & AMSR2 and SMOS & SMOS-SMAP results show a higher percentage of recurrence ($\geq$ 50%) along the entire coastline than SMMR, SSM/I & SSMIS. A similar situation can also be observed in the North East Water (NEW) and the East Siberian Sea. Despite the data resolution causing inconsistencies in the MIZ as mentioned above, this finding suggests that polynyas in those regions have occurred more frequently over the last two decades as AMSR-E & AMSR2 and SMOS & SMOS-SMAP satellite observations started after the 2000s. We therefore now conduct a temporal analysis of polynya activity.

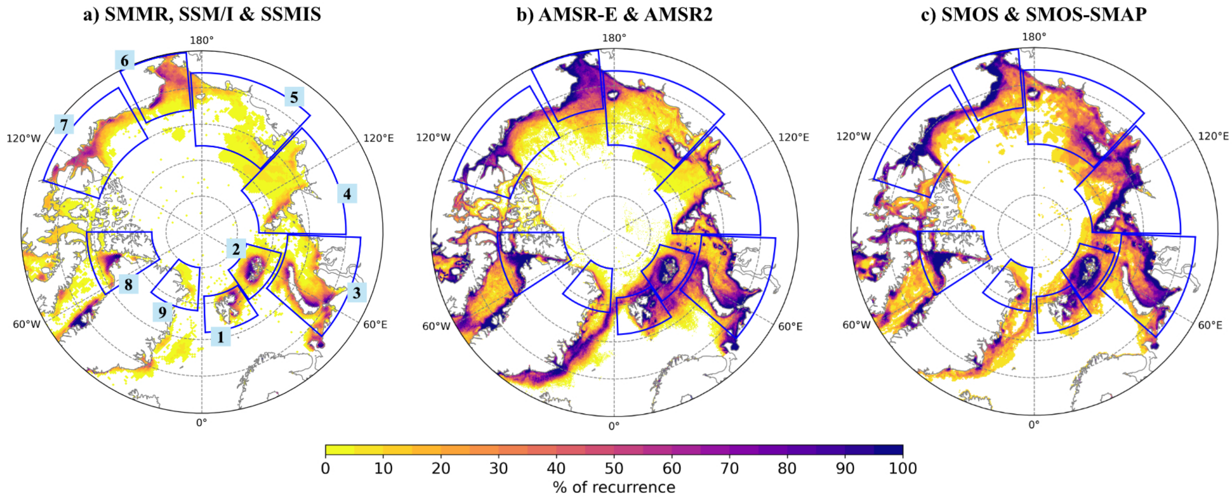

FIG. 3. Arctic polynya recurrence frequency for the three satellite datasets over their respective analysis period using a SIC threshold of 50% or SIT threshold of 20 cm. SMMR, SSM/I & SSMIS has as analysis period 1978-2024 (a); AMSR-E & AMSR2, 2002-2024 (b); SMOS & SMOS-SMAP, 2012-2024 (c). Blue boxed regions in (a) indicate our regions of interest for the next section's analysis; their numbers match the regions of Table 3.

b. Temporal variability and trends in winter polynyas, at the pan-Arctic and regional scales

The cumulative polynya number is inconsistent among the products (Figure 4a). The cumulative polynya number from the 6.25 km resolution AMSR-E & AMSR2 is continuously exceeding 100 000 (Fig 4a, turquoise). The SIT-based, 12.5 km resolution SMOS & SMOS-SMAP has a range of 10 000 to 14 000, constantly exceeding that of the SIC-based, 25 km resolution SMMR, SSM/I & SSMIS which fluctuates between 200 and 800 over their common time period (Figure 4a, orange and dark blue lines, respectively). This difference in the cumulative number caused by the resolution of the satellite products aligns with the differences in spatial distribution found in section 4a.

Both the total pan-Arctic winter polynya area and cumulative polynya area have an increasing trend for the past 47 years (Figure 4b and c). The total area of polynyas calculated from AMSR-E & AMSR2 and SMOS & SMOS-SMAP is around double that from SMMR, SSM/I & SSMIS, and the cumulative area is nearly 10 times larger (Figure 4b-c). It is logical that AMSR-E & AMSR2 and SMOS & SMOS-SMAP have larger area values than SMMR, SSM/I & SSMIS since more grid cells are identified as polynyas. Focusing on SMMR, SSM/I & SSMIS, which is the only timeseries with more than 20 years of uninterrupted results and therefore enhances the robustness of any trend analysis, we find a positive trend of 17.0×10^3 km^2 year^{-1} for the total polynya area, and 12.2×10^4 km^2 year^{-1} for the cumulative area (Table 3). However, we find no significant trend in the polynya number; this indicates that regions where polynyas form and the extent of the polynyas have expanded over the past four decades.

From section 4a, we suspect that the more intense recurrence signal for the two more recent datasets is due to more active polynya formation after the 2000s. From a pan-Arctic scale, the total area has a positive trend 19.4×10^3 km^2 year^{-1} over 1978/79 - 2000/01, after which the trend increases slightly to 20.9×10^3 km^2 year^{-1} over 2000/01 - 2023/24. The cumulative area has a larger increase over 1978/79 - 2000/01 (16.2×10^4 km^2 year^{-1}) than over 2000/01 - 2023/24 (10.0×10^4 km^2 year^{-1}). These results suggest that although more grid cells exhibit polynya activity in the last two decades, the increase in area extent slowed down since the 2000s.

TABLE 3. SMMR, SSM/I & SSMIS Arctic and regional winter polynya total area trend and cumulative area trend since 1978. All results are at or above the 90% statistically significant level.

Region	Total polynya area trend (10^3km^2 year^{-1})			Cumulative polynya area trend (10^4km^2 year^{-1})		
	1978/79 - 2023/24	1978/79 - 2000/01 (Period 1)	2000/01 - 2023/24 (Period 2)	1978/79 - 2023/24	1978/79 - 2000/01 (Period 1)	2000/01 - 2023/24 (Period 2)
Arctic	17.0	19.4	20.9	12.2	16.2	10.0
1. Svalbard	-	-	-	0.32	-	-
2. Franz Josef Land	2.26	2.24	1.81	2.59	2.67	-
3. Kara Sea	1.35	4.84	-	1.11	3.87	-
4. Laptev Sea	3.09	1.05	5.53	1.22	0.30	-
5. East Siberian Sea	1.92	-	4.74	0.44	-	1.18
6. Chukchi Sea	1.54	4.21	-	0.80	2.58	1.33
7. Beaufort Sea	3.45	3.57	-	2.30	1.80	-
8. North Open Water (NOW)	1.22	1.38	-	1.71	1.57	-
9. North East Water (NEW)	0.20	-	-	-	-	-

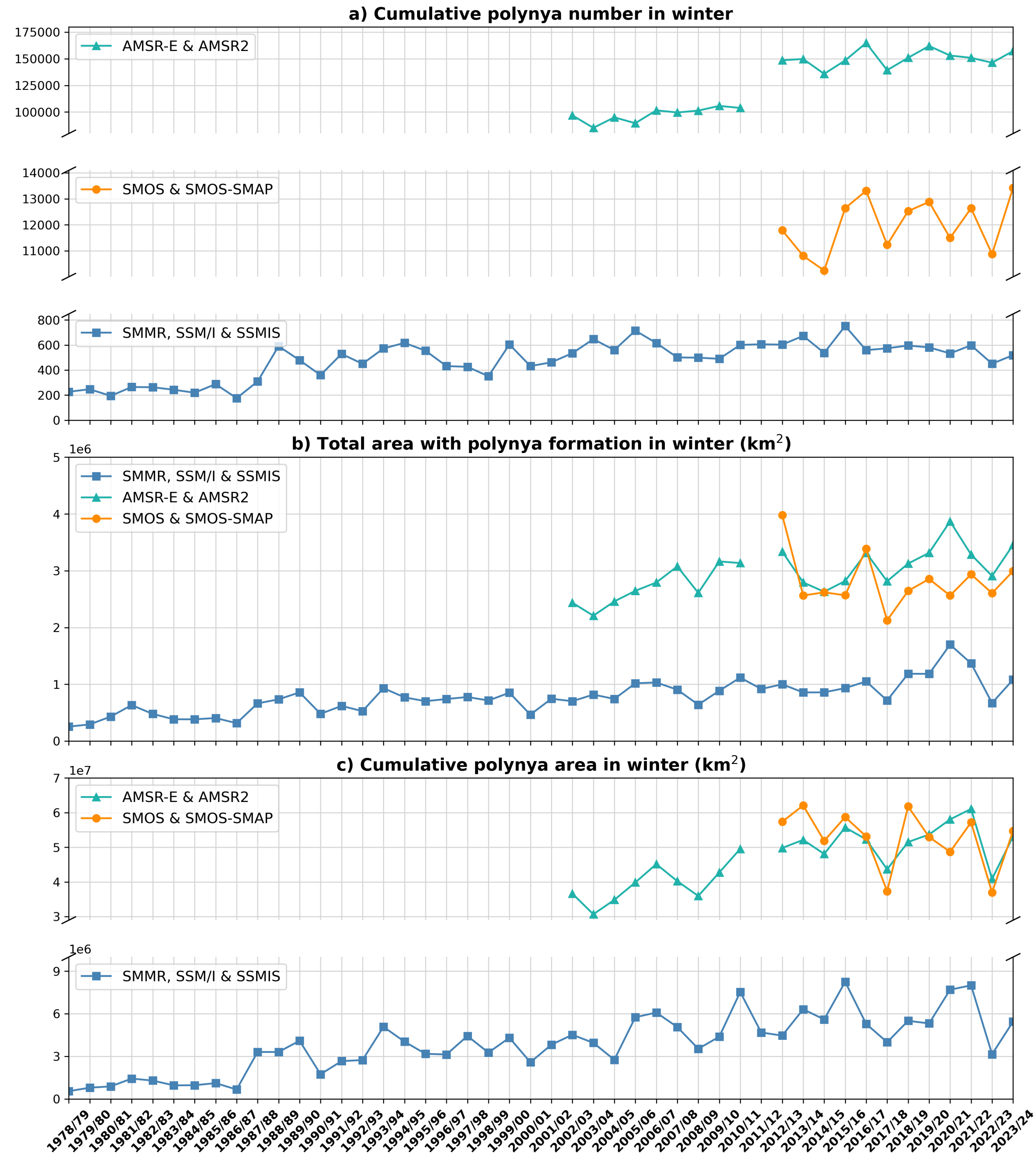

FIG. 4. Cumulative polynya number (a), total area with polynya formation (b) and cumulative polynya area (c) in winter from 1978 to 2024.

We hypothesise that the regional trends for the main polynyas may differ from each other based on our spatial findings (section 4a). We therefore define nine regions of interest, highlighted in Figure 3a; their locations are stated in the appendix Table A1. The Beaufort Sea (3.5×10^3 km^2 year^{-1}), Laptev Sea (3.1×10^3 km^2 year^{-1}) and Franz Josef Land (2.3×10^3 km^2 year^{-1}) have the largest increase in polynya area, and contribute to more than half of the increase in the pan-Arctic total polynya area trend (Table 3). As discussed previously, in section 4a we speculated that the larger recurrence values on two datasets are due to more active polynya formation after the 2000s. Yet when it comes to the trend differences before and after 2000, only the Laptev Sea and the East Siberian Sea show a higher increasing rate, approximately 5 times higher in total polynya area over the period 2000/01 - 2022/23. This may explain the more intense recurrence signal observed in the spatial distribution highlighted in section 4a (Figure 3b-c). In terms of the cumulative area, regions that contribute most to the trend are the Franz Josef Land (2.6×10^4 km^2 year^{-1}), Beaufort Sea (2.3×10^4 km^2 year^{-1}) and NOW (1.7×10^4 km^2 year^{-1}); however, they do not have an accelerated positive trend in their second period. Instead, the East Siberian Sea is the only region that has a higher increasing rate after the 2000s (1.2×10^4 km^2 year^{-1} over period 2; no significant trend over period 1, Table 3). We also find a decrease in the Chukchi Sea cumulative polynya area trend over the second period, and no trend existing in other regions after the 2000s. We now investigate the reasons for these apparently diverging results.

Most polynya regions have an increase in their polynya opening frequency of 1-2 times per decade, whereas Franz Josef Land and NOW show a more evident increase of more than 10 times per decade (Figure 5a). Regions with an increasing opening frequency have a positive trend of temperature or wind. For example, regions next to the Barents-Kara Sea have a significant increase in air temperature (T2m) of 1-3K and wind speed (WS) of 0.1-0.3 ms^{-1} per decade (Figure 5b-c). This is further shown in Table 4: the area-weighted mean T2m trend and recent studies have indicated that most Arctic regions have an increasing air temperature trend over the past few decades, especially for regions near the Atlantic Water inflow (e.g. Franz Josef Land, Kohnemann et al. 2017; Rantanen et al. 2022). The area-weighted WS trend is not statistically significant in all regions except the Kara Sea. Moving onto U10 and V10 at 90$^{\text{th}}$ percentile, there is a positive trend in the NEW for U10 and in the Kara Sea for V10. This strengthening of the southerly winds may be due to the higher frequency of winter extreme cyclone activity in the Eurasian sector in recent years (Rinke et al. 2017). Although area-weighted results do not have an evident trend for any of the wind variables in most regions, significant wind trends are present in some grid cells of the regions (Figure 5c-e). Besides, the strong positive trend in southerly winds exceeding 0.4 ms^{-1} per decade locally over the Kara Sea may be leading to increased opening frequency in the north of neighbouring Franz Josef Land (Figure 5a and e). Our results reveal that the WS trend is most pronounced on a local scale, suggesting that its effect may be more evident on local polynya opening instead of regional cumulative area.

TABLE 4. Area-weighted winter mean trend of all atmospheric drivers. All results are at or above 90% statistically significant level.

Region	Area-weighted winter mean trend (1978/79 - 2023/24)			
	T2m ($K\ year^{-1}$)	WS ($ms^{-1} year^{-1}$)	U10 90th Percentile ($ms^{-1} year^{-1}$)	V10 90th Percentile ($ms^{-1} year^{-1}$)
Arctic	0.08	-	-	-
1. Svalbard	0.14	-	-	-
2. Franz Josef Land	0.17	-	-	-
3. Kara Sea	0.13	0.01	-	0.01
4. Laptev Sea	0.11	-	-	-
5. East Siberian Sea	0.09	-	-	-
6. Chukchi Sea	0.08	-	-	-
7. Beaufort Sea	0.07	-	-	-
8. North Open Water (NOW)	0.04	-	-	-
9. North East Water (NEW)	0.04	-	0.01	-

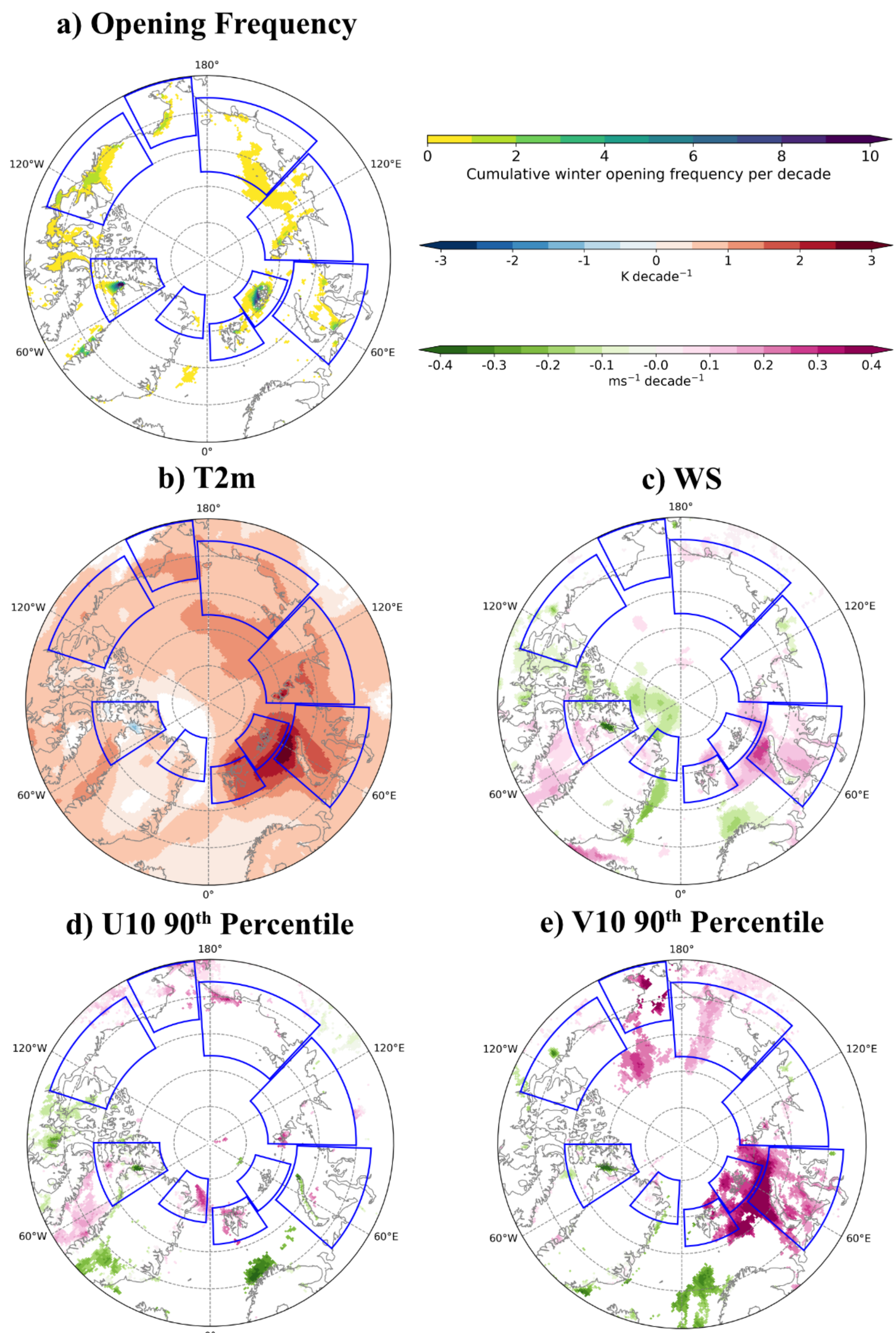

FIG. 5. The trend of (a) winter-cumulated opening frequency, (b) winter mean T2m, (c) winter mean WS, (d) winter mean U10 90th percentile and (e) winter mean V10 90th percentile. All results are at or above 90% statistically significant level.

Since we showed that the cumulative polynya area trend has a different trend before and after the 2000s, we finish the temporal analysis with an analysis of its monthly variability, and whether this variability has changed as well. The maximum cumulative polynya area usually occurs in November or April at the pan-Arctic scale but this varies across the different regions (Figure 6). The area is maximal in the early winter for regions on the Pacific side (East Siberian Sea, Chukchi Sea, and Beaufort Sea). For regions on the Atlantic side (Svalbard, Franz Josef Land, Kara Sea, NEW), their maximum months are more widely spread, but occur mainly in the mid or late winter. There is a shift of the month of maximum area after the 2000s, but the direction of the shift depends on the region. Most noticeably, in the Chukchi Sea, we find a one-month shift from November to December, while the others remain in November. Similarly there is a substantial shift of the maximum area month in NEW from early winter to late winter if polynyas are formed in the region, with only two occurrences (out of 10) after December in the first period, but 9 out of 15 after December in the second period. In the Laptev Sea in contrast, the maximum cumulative area occurs throughout winter before the 2000s, but it occurs more in November in recent years (11 out of 24 in period 2, compared to 5 out of 23 in period 1, Figure 6).

The different shifts in seasonality and trends in the different regions despite an overall warming Arctic suggests competing effects from the atmospheric drivers. We suspect that there may be a correlation between polynya events and atmospheric conditions; however, it is difficult to quantify the effect of the atmosphere on a winter-averaged timescale. Therefore, in the next section, we will examine the correlation from a daily-scale perspective.

c. Atmospheric forcings on polynya openings

We conduct a lagged correlation analysis between the on-off polynya state and the time series of the four potential drivers at the same location (air temperature in red, wind speed in orange, u- and v- winds in dark blue and turquoise, respectively, on Figure 7), counting for each region the number of grid cells where the correlation is maximal for that lag. The lagged correlation indicates that the wind has a more immediate impact on polynya openings compared to temperature. As expected, the effect of WS, U10, and V10 on polynya openings has a 1- to at most 2-day delay in most regions, whereas the instantaneous correlation (lag=0) is often at or close to 0 (Figure 7, orange, blue and green lines). The results align with the fact that most Arctic polynyas are mainly

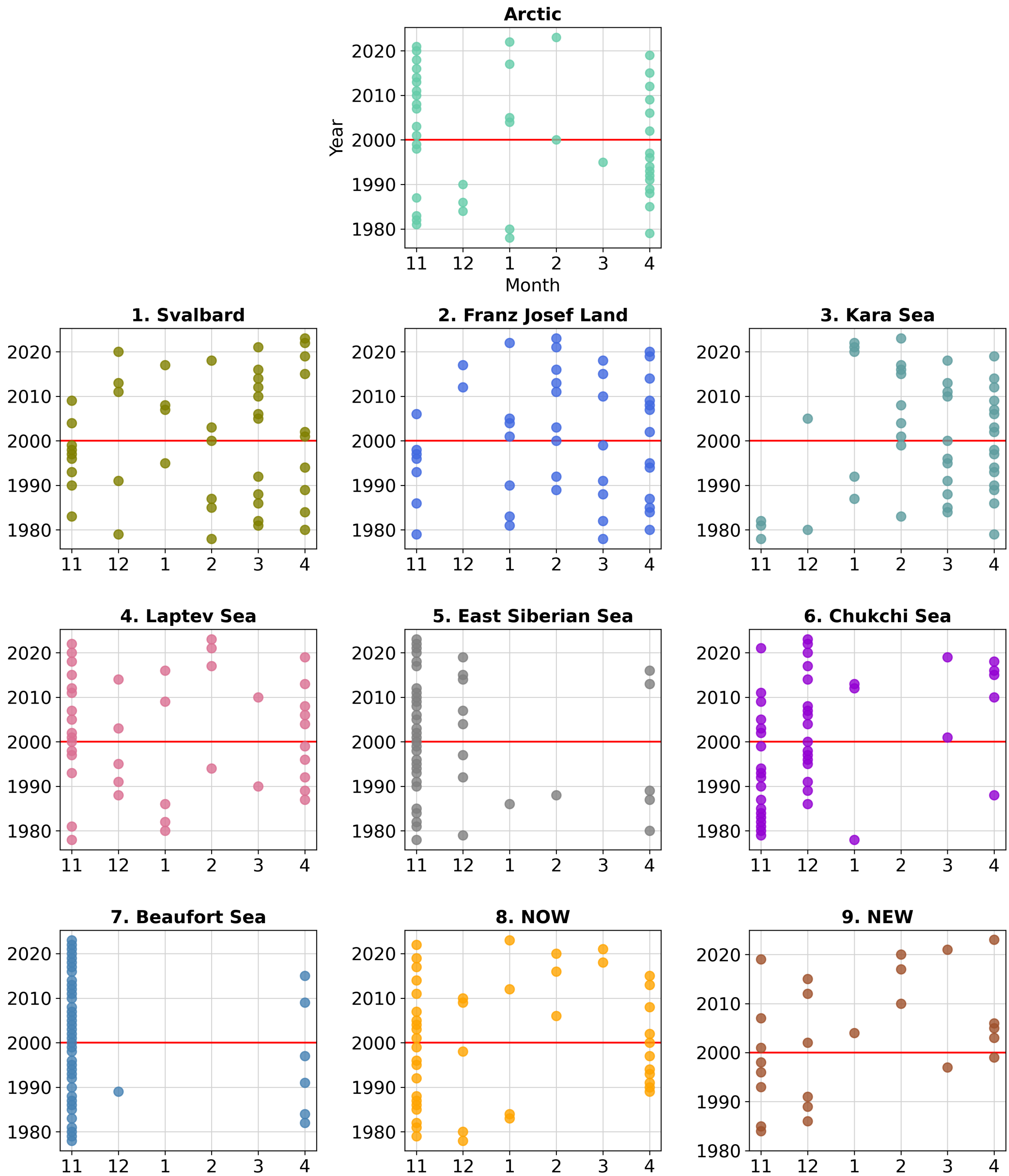

351 Fig. 6. The distribution of the maximum cumulative polynya area month from 1978 to 2024. Red line is the
352 cut-off year 2000. One dot represents one winter if there are polynyas formed in that winter.

coastal polynyas, and wind is a crucial driver forcing the ice cover to open. Meanwhile, the lag effect of air temperature on Arctic polynyas is more ambiguous (Figure 7, red lines). There is no notable difference between the Atlantic and Pacific sectors, but there are more grid cells with the highest correlation coefficient at 1-day lag in Franz Josef Land and NEW. For some regions such as Svalbard, Laptev Sea and Chukchi Sea, the T2m lag effect can even last up to 7 days; however, in Kara Sea, East Siberian Sea, Beaufort Sea and NOW, the highest correlation occurs instantaneously without time delay. The T2m effect on polynya openings remains uncertain as this high instantaneous correlation can imply that either warmer T2m favours polynya formation via increased surface melt, or that the opening of the ice cover in winter has an immediate impact on regional T2m.

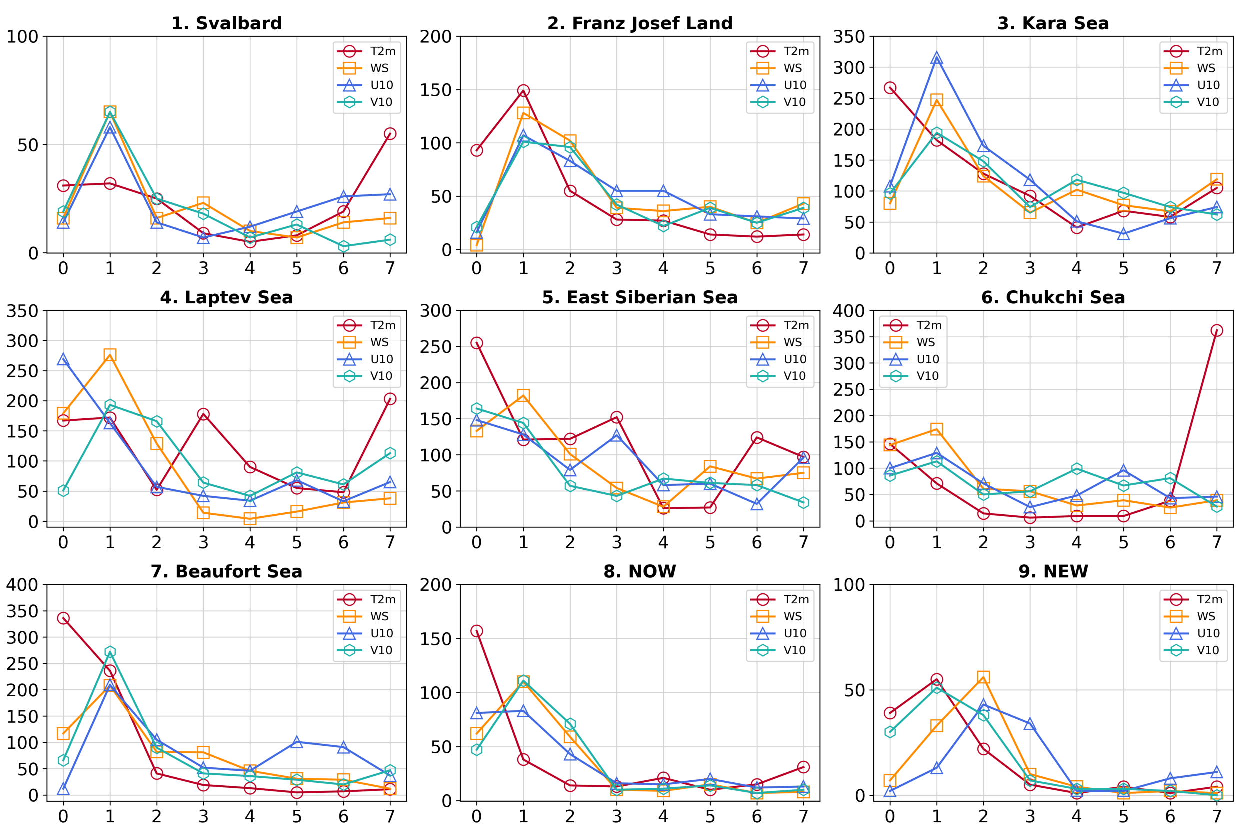

FIG. 7. Total grid counts of maximum absolute correlation coefficient between the on-off polynya state and the four potential atmospheric drivers: air temperature T2m in red; wind speed WS in orange; u- and v- component of wind U10 and V10 in dark blue and turquoise, respectively, in the nine regions of interest. X-axis is the number of days of lag tested, with the drivers being before the polynya state.

The actual values of these correlations are in Table 5, limiting our results to the first three days of lag only since we found the lag effect to be most prominent on the first or the second day (Figure 7). T2m is more positively correlated than WS in all regions according to the lagged correlation between atmospheric variables and daily total polynya area. From a pan-Arctic perspective, T2m correlation coefficients are higher than those of any wind parameters, regardless of the lag (Table 5 and A2). The correlation of T2m reaches up to 0.36 on lagged day 2 from a pan-Arctic scale but only 0.09 for V10 90th percentile, which implies that temperature has a prolonged effect on the polynya area extent. These results are consistent with the findings of Pease (1987) using an idealised polynya model: warmer temperature maximises and sustains the area extent of a polynya; both ice advection and ice production rates increase with wind speed, and yet large ice production rate also implies that newly formed ice will restrict the total extent. We obtain the same results on the regional scale, except for Franz Josef Land and NOW, where the T2m, WS and V10 90th percentile correlation coefficients are of similar magnitudes around 0.3 (Tables 5, and A2 to A5). We suggest that strong winds enhance the opening of the polynya, only if the temperature is also warm enough to suspend the ice production at the site; however, this hypothesis still has to be verified by modelling to understand the coupled effect of temperature and wind on the polynya development.

TABLE 5. Lagged correlation between the atmospheric variables and daily polynya area, with atmospheric variables first. All results are at or above 90% statistically significant level. Full lagged correlation tables can be found in appendix table A2, A3, A4 and A5.

Region	T2m			WS			U10 90th Percentile			V10 90th Percentile		
	Day 0	Day 1	Day2	Day 0	Day 1	Day 2	Day 0	Day 1	Day 2	Day 0	Day 1	Day 2
Arctic	0.35	0.36	0.36	0.06	0.07	0.06	0.06	0.05	0.05	0.07	0.08	0.09
1. Svalbard	0.06	0.07	0.07	-	0.03	0.03	0.09	0.10	0.09	-	-	-
2. Franz Josef Land	0.35	0.37	0.34	0.25	0.33	0.30	-0.04	-0.05	-0.04	0.20	0.28	0.29
3. Kara Sea	0.24	0.24	0.22	0.12	0.15	0.14	0.05	0.05	0.05	0.07	0.09	0.11
4. Laptev Sea	0.17	0.17	0.17	0.05	0.06	0.05	0.04	0.04	0.04	0.03	0.05	0.04
5. East Siberian Sea	0.12	0.13	0.13	0.05	0.06	0.04	-	-	-	-	-	-
6. Chukchi Sea	0.11	0.11	0.10	0.10	0.12	0.11	-0.06	-0.07	-0.06	-	-	-
7. Beaufort Sea	0.23	0.25	0.25	0.07	0.08	0.07	-0.05	-0.07	-0.07	0.05	0.05	0.04
8. North Open Water (NOW)	0.24	0.23	0.21	0.26	0.27	0.21	0.08	0.07	0.05	-0.08	-0.15	-0.14
9. North East Water (NEW)	0.11	0.11	0.11	0.06	0.07	0.07	-0.03	-0.05	-0.07	0.16	0.18	0.17

Finally, since a 1-day lag gave high correlations with both the wind variables and the air temperature in most regions, we finish with a brief investigation of the spatial pattern of this 1-day lagged correlation. We find a positive correlation between polynya opening and the previous day's T2m and WS (Figure 8a-b) for most of the major polynyas. T2m and WS have a similar positive correlation in NOW, Franz Josef Land and Chukchi Sea ($R \geq 0.3$, Figure 8a-b): the warmer or windier, the more the polynya is open. For regions with a high WS correlation, most polynya openings align with the wind direction from the continent to the Arctic region, as shown by the correlation with the two wind components (Figure 8c-d): Polynyas formed in the Barents-Kara Sea mainly correlate with V10 (wind from the Eurasian continent), while on the side of the Beaufort Sea and Chukchi Sea, polynyas depend on U10 (eastward wind along the Canadian archipelago). One exception is NOW, where winds flow parallel with the Nares Strait due to the channeling effect by the local topography, and thus polynya activity is more strongly correlated with V10 (correlations exceeding -0.3). Franz Josef Land is the only region that shows an evident correlation with all atmospheric drivers (Figure 8). Its 1-day lag result confirms that polynya openings in this region are triggered by both temperature and wind (Figure 7). Recalling Figure 5, the positive trend of opening frequency in Franz Josef Land may be explained by the rising near-surface temperature and strengthening northward wind events in the Barent-Kara Sea. These two regions also clearly exhibit dipoles in their correlations with the wind components (Figure 8c and d), negative in the south or west and positive in the north or east, consistent with findings from e.g. Tamura and Ohshima (2011) or Preußer et al. (2015) who showed enhanced ice production in the lee of the islands. On the other hand, wind is the dominant driver in NOW and the Chukchi Sea region, as shown in the 1-day lag analysis (Figure 8), where the Chukchi Sea region is more correlated with U10 while NOW is with V10. From Figure 5, the increasing opening trend in NOW aligns with the stronger northerly wind along the Nares Strait, whereas the weak opening frequency trend in the Chukchi Sea may be implied by the absence of wind trends in that area. In other major polynya regions, such as the Laptev Sea, Kara Sea, and the Beaufort Sea, T2m has a higher correlation than any other wind variables, and all T2m trends are positive (Table 4); however, the opening frequency trends are insignificant in those regions. These results imply that T2m may not be the crucial polynya driver, which also coincides with the ambiguous T2m lag results in Figure 7. Combining all the findings of polynya openings, we can conclude that wind plays a partial but significant role in most of the Arctic polynya formations, especially in major polynya areas, and that the inconsistent wind trends despite a clear Arctic air warming is the reason for the complex, non-linear polynya trends we quantified.

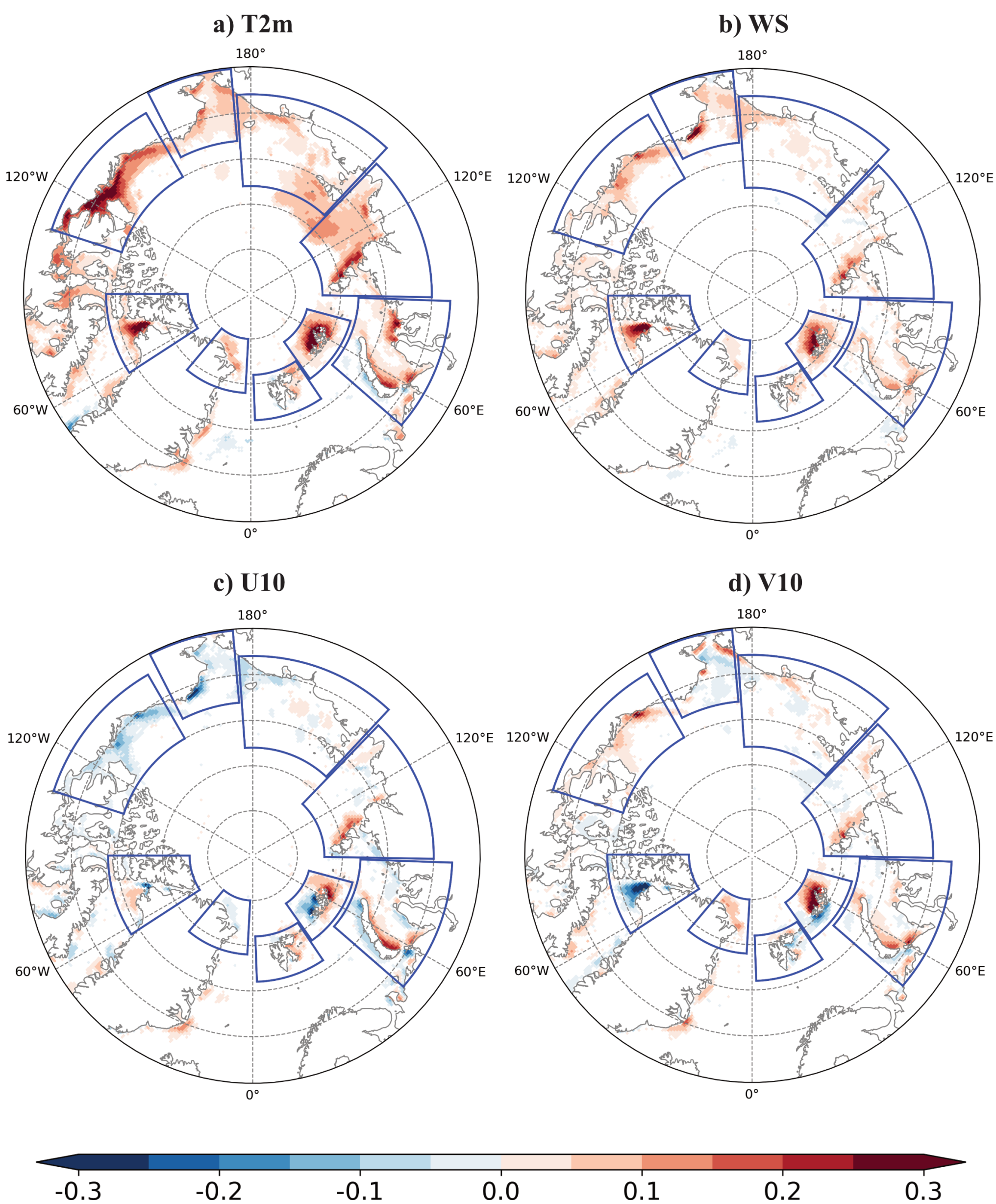

Fig. 8. 1-day lag correlation of on-off state with daily T2m (a), WS (b), U10 (c) and V10 (d). Coloured areas are at or above 90% significance level.

5. Conclusions

The main purpose of this study was to examine the spatial and temporal distribution of all Arctic polynyas that occurred in the past 47 years, with existing passive microwave satellite sea ice products. We also quantified the correlation between polynya events and atmospheric variables. Our main findings can be summarised as follows:

- Regardless of the sea ice product, the regions with the highest polynya recurrence are the western Laptev Sea, the western Kara Sea, Franz Josef Land, eastern Svalbard, North Open Water, the eastern Beaufort Sea and the Chukchi Sea. The retrieved area and polynya numbers are affected by the product's horizontal resolution, with high resolution resulting in noise in the marginal ice zone. For now, short time coverage and uncertainty in the data product limit the usefulness of the sea ice thickness retrievals.
- Both the total and cumulative winter polynya areas have an increasing trend in the Arctic of approximately 17000 km^2 $year^{-1}$ and 12000 km^2 $year^{-1}$ respectively over 1978 - 2024. Total winter polynya area is dominated by trends in the Laptev Sea, Franz Josef Land and the Beaufort Sea, whereas the cumulative area is more influenced by trends in the Franz Josef Land, Beaufort Sea and NOW.
- The correlation analysis indicates that wind speed is more related to the opening of a polynya, while the air temperature is strongly correlated with the polynya area. The effect of the wind speed and wind components has a 1- to 2- day lag while that of the air temperature can extend up to a 7-day lag.

Our results suggest that polynya activity will increase further as air temperatures continue to rise and extreme wind events become more frequent, particularly in some regions that already have a high recurrence signal of polynyas (Figure 5a). We acknowledge that the correlation coefficients of air temperature and wind on polynyas, although significant, are not large (Table 5, A2 to A5). This implies that polynyas are a complex natural phenomenon that cannot be explained by a single driver. As winter Arctic sea ice cover continues decreasing (Cavalieri and Parkinson 2012), Arctic polynyas may soon extend to the open-ocean where they would be affected by different drivers, both in the atmosphere and the ocean; their study might however become even more complex owing to data paucity in the open Arctic Ocean. Yet understanding the drivers and impacts of polynyas is not only beneficial for understanding their local effect on the climate, but is also a pre-requisite for accurate monitoring and projections of local biological activity, pan-Arctic air-sea exchanges of carbon and oxygen, and the global oceanic circulation.

Acknowledgments. This work was funded by the Swedish National Space Agency grant no. 2022-00149 awarded to CH. The computations were enabled by resources provided by the National Academic Infrastructure for Supercomputing in Sweden (NAISS), partially funded by the Swedish Research Council through grant agreement no. 2022-06725.

Data availability statement. The scripts for the polynya retrieval algorithm, using NSIDC SIC data as an example, are available on Github at `https://github.com/carmenwhm/Arctic_polynyas_paper`. The observed sea ice concentration data from the NSIDC are available at `https://nsidc.org/data/nsidc-0051/versions/2`, last accessed on 24 April 2025. The observed sea ice concentration and sea ice thickness data from the University of Bremen Sea Ice Remote Sensing group are available at `https://seaice.uni-bremen.de/start/`, last accessed on 24 April 2025. During peer-review, the daily polynya locations of SMMR, SSM/I & SSMIS and SMOS & SMOS-SMAP can be accessed at `https://www.dropbox.com/scl/fi/fr0barqpe519e1nu6kl3q/daily_location.nc?rlkey=zh1ganta0noexwvvvch4sh3zr&dl=1` and `https://www.dropbox.com/scl/fi/9a91cbsgrqj29o5ckb5zq/daily_location_SMOS.nc?rlkey=bdvlvay1k0rkql973u731ku0z&dl=1` respectively; they will be made publicly available closer to manuscript acceptance.

APPENDIX A

Full Regional Analysis Results

TABLE A1. Spatial information of nine regions of interest for lag correlation analysis.

Region	Lon, Lat
1. Svalbard	2°-34°E, 76°-81°N
2. Franz Josef Land	35°-73°E, 78.5°-83.5°N
3. Kara Sea	49°-88°E, 68°-78°N
4. Laptev Sea	89°-136°E, 70°-82°N
5. East Siberian Sea	137°E-176°W, 68°-78°N
6. Chukchi Sea	153°-175°W, 65°-73°N
7. Beaufort Sea	108°-150°W, 67°-75°N
8. North Open Water (NOW)	57°-90°W, 74°-83°N
9. North East Water (NEW)	3°-40°W, 79°-85°N

TABLE A2. Lag correlation results of T2m with daily polynya area. All results are at or above 90% statistically significant level.

Region	Day 0	Day 1	Day 2	Day 3	Day 4	Day 5	Day 6	Day 7
Arctic	0.35	0.36	0.36	0.37	0.37	0.36	0.36	0.35
1. Svalbard	0.06	0.07	0.07	0.06	0.05	0.04	0.04	0.04
2. Franz Josef Land	0.35	0.37	0.34	0.31	0.27	0.24	0.22	0.19
3. Kara Sea	0.24	0.24	0.22	0.19	0.17	0.14	0.12	0.10
4. Laptev Sea	0.17	0.17	0.17	0.17	0.17	0.17	0.17	0.17
5. East Siberian Sea	0.12	0.13	0.13	0.14	0.14	0.14	0.14	0.14
6. Chukchi Sea	0.11	0.11	0.10	0.10	0.09	0.09	0.10	0.10
7. Beaufort Sea	0.23	0.25	0.25	0.26	0.26	0.27	0.27	0.28
8. North Open Water (NOW)	0.24	0.23	0.21	0.20	0.19	0.17	0.17	0.16
9. North East Water (NEW)	0.11	0.11	0.11	0.10	0.08	0.08	0.06	0.06

TABLE A3. Lag correlation results of WS with daily polynya area. All results are at or above 90% statistically significant level.

Region	Day 0	Day 1	Day 2	Day 3	Day 4	Day 5	Day 6	Day 7
Arctic	0.06	0.07	0.06	0.04	-	-	-0.04	-0.04
1. Svalbard	-	0.03	0.03	0.02	-	-	-	-
2. Franz Josef Land	0.25	0.33	0.30	0.25	0.19	0.15	0.12	0.11
3. Kara Sea	0.12	0.15	0.14	0.11	0.09	0.06	0.03	-
4. Laptev Sea	0.05	0.06	0.05	0.03	-	-	-	-
5. East Siberian Sea	0.05	0.06	0.04	0.03	-	-	-	-
6. Chukchi Sea	0.10	0.12	0.11	0.09	0.08	0.06	0.04	0.02
7. Beaufort Sea	0.07	0.08	0.07	0.07	0.06	0.06	0.06	0.06
8. North Open Water (NOW)	0.26	0.27	0.21	0.15	0.11	0.08	0.05	0.05
9. North East Water (NEW)	0.06	0.07	0.07	0.05	0.02	-	-	-

Table A4. Lag correlation results of U10 90^{th} Percentile with daily polynya area. All results are at or above 90% statistically significant level.

Region	Day 0	Day 1	Day 2	Day 3	Day 4	Day 5	Day 6	Day 7
Arctic	0.06	0.05	0.05	0.04	0.03	0.03	0.03	0.03
1. Svalbard	0.09	0.10	0.09	0.07	0.07	0.09	0.09	0.09
2. Franz Josef Land	-0.04	-0.05	-0.04	-0.02	-	-	-	-
3. Kara Sea	0.05	0.05	0.05	0.04	0.02	-	-	-
4. Laptev Sea	0.04	0.04	0.04	0.04	0.04	0.04	0.03	0.04
5. East Siberian Sea	-	-	-	-	-0.02	-0.03	-0.03	-0.02
6. Chukchi Sea	-0.06	-0.07	-0.06	-0.04	-0.03	-	-	-
7. Beaufort Sea	-0.05	-0.07	-0.07	-0.07	-0.07	-0.08	-0.07	-0.07
8. North Open Water (NOW)	0.08	0.07	0.05	0.03	0.03	-	-	-
9. North East Water (NEW)	-0.03	-0.05	-0.07	-0.07	-0.05	-0.04	-0.02	-0.02

Table A5. Lag correlation results of V10 90^{th} Percentile with daily polynya area. All results are at or above 90% statistically significant level.

Region	Day 0	Day 1	Day 2	Day 3	Day 4	Day 5	Day 6	Day 7
Arctic	0.07	0.08	0.09	0.07	0.06	0.04	0.03	0.03
1. Svalbard	-	-	-	-	-	-	-	0.02
2. Franz Josef Land	0.20	0.28	0.29	0.28	0.25	0.22	0.19	0.18
3. Kara Sea	0.07	0.09	0.11	0.10	0.09	0.09	0.08	0.05
4. Laptev Sea	0.03	0.05	0.04	0.03	-	-	-	-
5. East Siberian Sea	-	-	-	0.02	-	-	-	-
6. Chukchi Sea	-	-	-	-	-0.03	-0.03	-	-
7. Beaufort Sea	0.05	0.05	0.04	0.03	0.03	0.02	0.02	0.03
8. North Open Water (NOW)	-0.08	-0.15	-0.14	-0.11	-0.09	-0.07	-0.05	-0.04
9. North East Water (NEW)	0.16	0.18	0.17	0.14	0.11	0.10	0.08	0.07

References

Aagaard, K., L. Coachman, and E. Carmack, 1981: On the halocline of the arctic ocean. *Deep Sea Research Part A. Oceanographic Research Papers*, **28 (6)**, 529–545, https://doi.org/https://doi.org/10.1016/0198-0149(81)90115-1, URL https://www.sciencedirect.com/science/article/pii/0198014981901151.

Adams, S., S. Willmes, D. Schröder, G. Heinemann, M. Bauer, and T. Krumpen, 2013: Improvement and sensitivity analysis of thermal thin-ice thickness retrievals. *IEEE Transactions on Geoscience and Remote Sensing*, **51 (6)**, 3306–3318, https://doi.org/10.1109/TGRS.2012.2219539.

Bareiss, J., and K. Görgen, 2005: Spatial and temporal variability of sea ice in the laptev sea: Analyses and review of satellite passive-microwave data and model results, 1979 to 2002. *Global and Planetary Change*, **48 (1)**, 28–54, https://doi.org/https://doi.org/10.1016/j.gloplacha.2004.12.004, URL https://www.sciencedirect.com/science/article/pii/S0921818105000573, arctic Siberian Shelf Environments.

Bennett, M. G., I. A. Renfrew, D. P. Stevens, and G. W. K. Moore, 2024: The northeast water polynya, greenland: Climatology, atmospheric forcing and ocean response. *Journal of Geophysical Research: Oceans*, **129 (5)**, e2023JC020 513, https://doi.org/https://doi.org/10.1029/2023JC020513, URL https://agupubs.onlinelibrary.wiley.com/doi/abs/10.1029/2023JC020513, e2023JC020513 2023JC020513, https://agupubs.onlinelibrary.wiley.com/doi/pdf/10.1029/2023JC020513.

Bliss, A. C., and M. R. Anderson, 2018: Arctic sea ice melt onset timing from passive microwave-based and surface air temperature-based methods. *Journal of Geophysical Research: Atmospheres*, **123 (17)**, 9063–9080, https://doi.org/https://doi.org/10.1029/2018JD028676, URL https://agupubs.onlinelibrary.wiley.com/doi/abs/10.1029/2018JD028676, https://agupubs.onlinelibrary.wiley.com/doi/pdf/10.1029/2018JD028676.

Boisvert, L. N., T. Markus, C. L. Parkinson, and T. Vihma, 2012: Moisture fluxes derived from eos aqua satellite data for the north water polynya over 2003–2009. *Journal of Geophysical Research: Atmospheres*, **117 (D6)**, https://doi.org/https://doi.org/10.1029/2011JD016949, URL https://agupubs.onlinelibrary.wiley.com/doi/abs/10.1029/2011JD016949, https://agupubs.onlinelibrary.wiley.com/doi/pdf/10.1029/2011JD016949.

Campbell, E., E. Wilson, G. Moore, S. Riser, C. Brayton, M. Mazloff, and L. Talley, 2019: Antarctic offshore polynyas linked to southern hemisphere climate anomalies. *Nature*, **570**, 1–7, https://doi.org/10.1038/s41586-019-1294-0.

Cavalieri, D. J., P. Gloersen, and W. J. Campbell, 1984: Determination of sea ice parameters with the nimbus 7 smmr. *Journal of Geophysical Research: Atmospheres*, **89 (D4)**, 5355–5369, https://doi.org/https://doi.org/10.1029/JD089iD04p05355, URL https://agupubs.onlinelibrary.wiley.com/doi/abs/10.1029/JD089iD04p05355, https://agupubs.onlinelibrary.wiley.com/doi/pdf/10.1029/JD089iD04p05355.

Cavalieri, D. J., and S. Martin, 1994: The contribution of alaskan, siberian, and canadian coastal polynyas to the cold halocline layer of the arctic ocean. *Journal of Geophysical Research: Oceans*, **99 (C9)**, 18 343–18 362, https://doi.org/https://doi.org/10.1029/94JC01169, URL https://agupubs.onlinelibrary.wiley.com/doi/abs/10.1029/94JC01169, https://agupubs.onlinelibrary.wiley.com/doi/pdf/10.1029/94JC01169.

Cavalieri, D. J., and C. L. Parkinson, 2012: Arctic sea ice variability and trends, 1979-2010. *The Cryosphere*, **6 (4)**, 881–889, https://doi.org/10.5194/tc-6-881-2012, URL https://tc.copernicus.org/articles/6/881/2012/.

Cavalieri, D. J., C. L. Parkinson, P. Gloersen, J. C. Comiso, and H. J. Zwally, 1999: Deriving long-term time series of sea ice cover from satellite passive-microwave multisensor data sets. *Journal of Geophysical Research*, **104 (C7)**, 15,803–15,814, https://doi.org/10.1029/1999JC900081.

Comiso, J. C., D. J. Cavalieri, C. L. Parkinson, and P. Gloersen, 1997: Passive microwave algorithms for sea ice concentration: A comparison of two techniques. *Remote Sensing of Environment*, **60 (3)**, 357–384, https://doi.org/https://doi.org/10.1016/S0034-4257(96)00220-9, URL https://www.sciencedirect.com/science/article/pii/S0034425796002209.

Dokken, S., P. Winsor, T. Markus, J. Askne, and G. Björk, 2002: Ers sar characterization of coastal polynyas in the arctic and comparison with ssm/i and numerical model investigations. *Remote Sensing of Environment*, **80**, 321–335, https://doi.org/10.1016/S0034-4257(01)00313-3.

Else, B. G. T., T. N. Papakyriakou, M. G. Asplin, D. G. Barber, R. J. Galley, L. A. Miller, and A. Mucci, 2013: Annual cycle of air-sea co2 exchange in an arctic polynya region. *Global Biogeochemical Cycles*, **27 (2)**, 388–398, https://doi.org/https://doi.org/10.1002/gbc.20016, URL https://agupubs.onlinelibrary.wiley.com/doi/abs/10.1002/gbc.20016, https://agupubs.onlinelibrary.wiley.com/doi/pdf/10.1002/gbc.20016.

Gordon, A. L., and J. C. Comiso, 1988: Polynyas in the southern ocean. *Scientific American*, **258 (6)**, 90–97, URL http://www.jstor.org/stable/24989126.

Gultepe, I., G. Isaac, A. Williams, D. Marcotte, and K. Strawbridge, 2003: Turbulent heat fluxes over leads and polynyas and their effects on arctic clouds during fire.ace: Aircraft observations for april 1998. *Atmosphere-ocean*, **41**, 15–34, https://doi.org/10.3137/ao.410102.

Hersbach, H., and Coauthors, 2020: The era5 global reanalysis. *Quarterly Journal of the Royal Meteorological Society*, **146 (730)**, 1999–2049, https://doi.org/https://doi.org/10.1002/qj.3803, URL https://rmets.onlinelibrary.wiley.com/doi/abs/10.1002/qj.3803, https://rmets.onlinelibrary.wiley.com/doi/pdf/10.1002/qj.3803.

Hirano, D., and Coauthors, 2016: A wind-driven, hybrid latent and sensible heat coastal polynya off barrow, alaska. *Journal of Geophysical Research: Oceans*, **121 (1)**, 980–997, https://doi.org/https://doi.org/10.1002/2015JC011318, URL https://agupubs.onlinelibrary.wiley.com/doi/abs/10.1002/2015JC011318, https://agupubs.onlinelibrary.wiley.com/doi/pdf/10.1002/2015JC011318.

Huntemann, M., G. Heygster, L. Kaleschke, T. Krumpen, M. Mäkynen, and M. Drusch, 2014: Empirical sea ice thickness retrieval during the freeze-up period from smos high incident angle observations. *The Cryosphere*, **8 (2)**, 439–451, https://doi.org/10.5194/tc-8-439-2014, URL https://tc.copernicus.org/articles/8/439/2014/.

Ingram, R., J. Bâcle, D. G. Barber, Y. Gratton, and H. Melling, 2002: An overview of physical processes in the north water. *Deep Sea Research Part II: Topical Studies in Oceanography*, **49 (22)**, 4893–4906, https://doi.org/https://doi.org/10.1016/S0967-0645(02)00169-8, URL https://www.sciencedirect.com/science/article/pii/S0967064502001698, the International North Water Polynya Study.

Iwamoto, K., K. I. Ohshima, and T. Tamura, 2014: Improved mapping of sea ice production in the arctic ocean using amsr-e thin ice thickness algorithm. *Journal of Geophysical Re-*

search: Oceans, **119 (6)**, 3574–3594, https://doi.org/https://doi.org/10.1002/2013JC009749, URL https://agupubs.onlinelibrary.wiley.com/doi/abs/10.1002/2013JC009749, https://agupubs.onlinelibrary.wiley.com/doi/pdf/10.1002/2013JC009749.

Kaleschke, L., X. Tian-Kunze, N. Maaß, M. Mäkynen, and M. Drusch, 2012: Sea ice thickness retrieval from smos brightness temperatures during the arctic freeze-up period. *Geophysical Research Letters*, **39 (5)**, https://doi.org/https://doi.org/10.1029/2012GL050916, URL https://agupubs.onlinelibrary.wiley.com/doi/abs/10.1029/2012GL050916, https://agupubs.onlinelibrary.wiley.com/doi/pdf/10.1029/2012GL050916.

Kawaguchi, Y., T. Tamura, S. Nishino, T. Kikuchi, M. Itoh, and H. Mitsudera, 2011: Numerical study of winter water formation in the chukchi sea: Roles and impacts of coastal polynyas. *Journal of Geophysical Research: Oceans*, **116 (C7)**, https://doi.org/https://doi.org/10.1029/2010JC006606, URL https://agupubs.onlinelibrary.wiley.com/doi/abs/10.1029/2010JC006606, https://agupubs.onlinelibrary.wiley.com/doi/pdf/10.1029/2010JC006606.

Kohnemann, S. H. E., G. Heinemann, D. H. Bromwich, and O. Gutjahr, 2017: Extreme warming in the kara sea and barents sea during the winter period 2000–16. *Journal of Climate*, **30**, 8913–8927, URL https://api.semanticscholar.org/CorpusID:134619123.

Marchese, C., C. Albouy, J.-É. Tremblay, D. Dumont, F. d'Ortenzio, S. Vissault, and S. Bélanger, 2017: Changes in phytoplankton bloom phenology over the North Water (NOW) polynya: a response to changing environmental conditions. *Polar Biology*, **40 (9)**, 1721–1737, https://doi.org/10.1007/s00300-017-2095-2, URL https://hal.science/hal-03136905.

Markus, T., J. C. Stroeve, and J. Miller, 2009: Recent changes in arctic sea ice melt onset, freezeup, and melt season length. *Journal of Geophysical Research: Oceans*, **114 (C12)**, https://doi.org/https://doi.org/10.1029/2009JC005436, URL https://agupubs.onlinelibrary.wiley.com/doi/abs/10.1029/2009JC005436, https://agupubs.onlinelibrary.wiley.com/doi/pdf/10.1029/2009JC005436.

Martin, S., and D. J. Cavalieri, 1989: Contributions of the siberian shelf polynyas to the arctic ocean intermediate and deep water. *Journal of Geophysical Research: Oceans*, **94 (C9)**, 12 725–12 738, https://doi.org/https://doi.org/10.1029/JC094iC09p12725, URL https://agupubs.onlinelibrary.wiley.com/doi/abs/10.1029/JC094iC09p12725, https://agupubs.onlinelibrary.wiley.com/doi/pdf/10.1029/JC094iC09p12725.

Martin, S., R. Drucker, R. Kwok, and B. Holt, 2004: Estimation of the thin ice thickness and heat flux for the chukchi sea alaskan coast polynya from special sensor microwave/imager data, 1990–2001. *Journal of Geophysical Research: Oceans*, **109 (C10)**, https://doi.org/https://doi.org/10.1029/2004JC002428, URL https://agupubs.onlinelibrary.wiley.com/doi/abs/10.1029/2004JC002428, https://agupubs.onlinelibrary.wiley.com/doi/pdf/10.1029/2004JC002428.

Massom, R. A., P. Harris, K. J. Michael, and M. Potter, 1998: The distribution and formative processes of latent-heat polynyas in east antarctica. *Annals of Glaciology*, **27**, 420–426, https://doi.org/10.3189/1998AoG27-1-420-426.

Mohrmann, M., C. Heuzé, and S. Swart, 2021: Southern ocean polynyas in cmip6 models. *The Cryosphere*, **15 (9)**, 4281–4313, https://doi.org/10.5194/tc-15-4281-2021, URL https://tc.copernicus.org/articles/15/4281/2021/.

Monroe, E. E., P. C. Taylor, and L. N. Boisvert, 2021: Arctic cloud response to a perturbation in sea ice concentration: The north water polynya. *Journal of Geophysical Research: Atmospheres*, **126 (16)**, e2020JD034 409, https://doi.org/https://doi.org/10.1029/2020JD034409, URL https://agupubs.onlinelibrary.wiley.com/doi/abs/10.1029/2020JD034409, e2020JD034409 2020JD034409, https://agupubs.onlinelibrary.wiley.com/doi/pdf/10.1029/2020JD034409.

Moore, G., S. Howell, and M. Brady, 2023: Evolving relationship of nares strait ice arches on sea ice along the strait and the north water, the arctic's most productive polynya. *Scientific Reports*, **13**, https://doi.org/10.1038/s41598-023-36179-0.

Morales Maqueda, M. A., A. J. Willmott, and N. R. T. Biggs, 2004: Polynya dynamics: a review of observations and modeling. *Reviews of Geophysics*, **42 (1)**, https://doi.org/https://doi.org/10.1029/2002RG000116, URL https://agupubs.onlinelibrary.wiley.com/doi/abs/10.1029/2002RG000116, https://agupubs.onlinelibrary.wiley.com/doi/pdf/10.1029/2002RG000116.

Nakata, K., K. I. Ohshima, S. Nihashi, N. Kimura, and T. Tamura, 2015: Variability and ice production budget in the ross ice shelf polynya based on a simplified polynya model and satellite observations. *Journal of Geophysical Research: Oceans*, **120 (9)**, 6234–6252, https://doi.org/https://doi.org/10.1002/2015JC010894, URL https://agupubs.onlinelibrary.wiley.com/doi/abs/10.1002/2015JC010894, https://agupubs.onlinelibrary.wiley.com/doi/pdf/10.1002/2015JC010894.

NSIDC, 2024: Summary of smmr, ssm/i and ssmis sensors. NASA National Snow and Ice Data Center Distributed Active Archive Center, URL https://nsidc.org/sites/default/files/documents/technical-reference/smmr-ssmi-ssmis-sensors.pdf.

Paţilea, C., G. Heygster, M. Huntemann, and G. Spreen, 2019: Combined smap–smos thin sea ice thickness retrieval. *The Cryosphere*, **13 (2)**, 675–691, https://doi.org/10.5194/tc-13-675-2019, URL https://tc.copernicus.org/articles/13/675/2019/.

Pease, C. H., 1987: The size of wind-driven coastal polynyas. *Journal of Geophysical Research: Oceans*, **92 (C7)**, 7049–7059, https://doi.org/https://doi.org/10.1029/JC092iC07p07049, URL https://agupubs.onlinelibrary.wiley.com/doi/abs/10.1029/JC092iC07p07049, https://agupubs.onlinelibrary.wiley.com/doi/pdf/10.1029/JC092iC07p07049.

Preußer, A., G. Heinemann, S. Willmes, and S. Paul, 2016: Circumpolar polynya regions and ice production in the arctic: results from modis thermal infrared imagery from 2002/2003 to 2014/2015 with a regional focus on the laptev sea. *The Cryosphere*, **10 (6)**, 3021–3042, https://doi.org/10.5194/tc-10-3021-2016, URL https://tc.copernicus.org/articles/10/3021/2016/.

Preußer, A., S. Willmes, G. Heinemann, and S. Paul, 2015: Thin-ice dynamics and ice production in the storfjorden polynya for winter seasons 2002/2003–2013/2014 using modis thermal infrared imagery. *The Cryosphere*, **9 (3)**, 1063–1073, https://doi.org/10.5194/tc-9-1063-2015, URL https://tc.copernicus.org/articles/9/1063/2015/.

Rantanen, M., A. Y. Karpechko, A. Lipponen, K. Nordling, O. Hyvärinen, K. Ruosteenoja, T. Vihma, and A. Laaksonen, 2022: The Arctic has warmed nearly four times faster than the globe since 1979. *Communications Earth and Environment*, **3 (1)**, 168, https://doi.org/10.1038/s43247-022-00498-3.

Ren, H., M. Shokr, X. Li, Z. Zhang, F. Hui, and X. Cheng, 2022: Estimation of sea ice production in the north water polynya based on ice arch duration in winter during 2006–2019.

Journal of Geophysical Research: Oceans, **127 (10)**, e2022JC018 764, https://doi.org/https://doi.org/10.1029/2022JC018764, URL https://agupubs.onlinelibrary.wiley.com/doi/abs/10.1029/2022JC018764, e2022JC018764 2022JC018764, https://agupubs.onlinelibrary.wiley.com/doi/pdf/10.1029/2022JC018764.

Rinke, A., M. Maturilli, R. Graham, H. Matthes, D. Handorf, L. Cohen, S. Hudson, and J. Moore, 2017: Extreme cyclone events in the arctic: Wintertime variability and trends. *Environmental Research Letters*, **12**, 094 006, https://doi.org/10.1088/1748-9326/aa7def.

Rolph, R. J., D. L. Feltham, and D. Schröder, 2020: Changes of the arctic marginal ice zone during the satellite era. *The Cryosphere*, **14 (6)**, 1971–1984, https://doi.org/10.5194/tc-14-1971-2020, URL https://tc.copernicus.org/articles/14/1971/2020/.

Shen, X., C.-Q. Ke, B. Cheng, W. Xia, L. Mengmeng, X. Yu, and H. Li, 2021: Thinner sea ice contribution to the remarkable polynya formation north of greenland in august 2018. *Advances in Atmospheric Sciences*, **38**, 1474–1485, https://doi.org/10.1007/s00376-021-0136-9.

Smedsrud, L. H., W. P. Budgell, A. D. Jenkins, and B. Ådlandsvik, 2006: Fine-scale sea-ice modelling of the Storfjorden polynya, Svalbard. *Annals of Glaciology*, **44 (1)**, 73–79, https://doi.org/10.3189/172756406781811295.

Smith, S. D., R. D. Muench, and C. H. Pease, 1990: Polynyas and leads: An overview of physical processes and environment. *Journal of Geophysical Research: Oceans*, **95 (C6)**, 9461–9479, https://doi.org/https://doi.org/10.1029/JC095iC06p09461, URL https://agupubs.onlinelibrary.wiley.com/doi/abs/10.1029/JC095iC06p09461, https://agupubs.onlinelibrary.wiley.com/doi/pdf/10.1029/JC095iC06p09461.

Spreen, G., L. Kaleschke, and G. Heygster, 2008: Sea ice remote sensing using amsr-e 89-ghz channels. *Journal of Geophysical Research: Oceans*, **113 (C2)**, https://doi.org/https://doi.org/10.1029/2005JC003384, URL https://agupubs.onlinelibrary.wiley.com/doi/abs/10.1029/2005JC003384, https://agupubs.onlinelibrary.wiley.com/doi/pdf/10.1029/2005JC003384.

Tamura, T., and K. I. Ohshima, 2011: Mapping of sea ice production in the arctic coastal polynyas. *Journal of Geophysical Research: Oceans*, **116 (C7)**, https://doi.org/https://doi.org/10.1029/

2010JC006586, URL https://agupubs.onlinelibrary.wiley.com/doi/abs/10.1029/2010JC006586, https://agupubs.onlinelibrary.wiley.com/doi/pdf/10.1029/2010JC006586.

Tian-Kunze, X., L. Kaleschke, N. Maaß, M. Mäkynen, N. Serra, M. Drusch, and T. Krumpen, 2014: Smos-derived thin sea ice thickness: algorithm baseline, product specifications and initial verification. *The Cryosphere*, **8 (3)**, 997–1018, https://doi.org/10.5194/tc-8-997-2014, URL https://tc.copernicus.org/articles/8/997/2014/.

Virtanen, P., and Coauthors, 2020: SciPy 1.0: Fundamental Algorithms for Scientific Computing in Python. *Nature Methods*, **17**, 261–272, https://doi.org/10.1038/s41592-019-0686-2.

Willmes, S., S. Adams, D. Schröder, and G. Heinemann, 2011: Spatio-temporal variability of polynya dynamics and ice production in the laptev sea between the winters of 1979/80 and 2007/08. *Polar Research*, https://doi.org/10.3402/polar.v30i0.5971, URL https://polarresearch.net/index.php/polar/article/view/3064.

Zhou, L., C. Heuzé, and M. Mohrmann, 2022: Early winter triggering of the maud rise polynya. *Geophysical Research Letters*, **49 (2)**, e2021GL096 246, https://doi.org/https://doi.org/10.1029/2021GL096246, URL https://agupubs.onlinelibrary.wiley.com/doi/abs/10.1029/2021GL096246, e2021GL096246 2021GL096246, https://agupubs.onlinelibrary.wiley.com/doi/pdf/10.1029/2021GL096246.